Sensitizing effects of $BiVO_4$ and visible light induced production of highly reductive electrons in the $TiO_2/BiVO_4$ heterojunction

Annalisa Polo, Ivan Grigioni, Maria Vittoria Dozzi, Elena Selli*

Dipartimento di Chimica, Università degli Studi di Milano, via Golgi 19, I-20133 Milano, Italy

A B S T R A C T

$BiVO_4$ is an efficient and stable visible active photoanode material. However, due to its unfavorable conduction band position which falls below the H_2 reduction potential, it fails to carry out the complete water splitting reaction. On the other hand, larger band gap TiO_2 is able to photocatalytically split water, thanks to its negative conduction band energy. Aiming at verifying the possibility of sensitizing TiO_2 with $BiVO_4$ and employing the so obtained composite material in photocatalytic water splitting under visible light, we prepared and photoelectrochemically characterized $TiO_2/BiVO_4$ heterojunction electrodes. The photocatalytic reduction of methyl viologen, an electron acceptor probe with a reduction potential close to that of protons, was used to evaluate the reducing ability of the photoactive materials under visible light. An apparently counterintuitive electron transfer from photoexcited $BiVO_4$ to the TiO_2 conduction band occurs in the $TiO_2/BiVO_4$ heterojunction, resulting in TiO_2 sensitization and production of highly reductive electrons, which appears to be favored by the band alignment occurring at the heterojunction.

Keywords: TiO_2, $BiVO_4$, heterojunction, visible light sensitization, methyl viologen reduction, photo(electro)catalysis

* Corresponding author at: Dipartimento di Chimica, Università degli Studi di Milano, via Golgi 19, I-20133 Milano, Italy. Tel.: +39 02 503 14237; fax: +39 02 503 14300.
E-mail address: elena.selli@unimi.it

1. Introduction

Collecting and storing solar energy into chemical bonds, mimicking nature in photosynthesis, is a highly desirable approach to face the global energy challenge [1–4]. In particular, overall water splitting under sunlight to produce clean hydrogen from a renewable source has attracted increasing attention in the last decades. Since the discovery of Fujishima and Honda in the early 1970s [5], photocatalytic and photoelectrochemical (PEC) water splitting on semiconducting materials has emerged as a promising strategy to produce solar hydrogen [6,7]. Solar fuels generated by the light-to-chemical energy conversion in PEC cells may play an important role towards a sustainable energy society, since they are storable, easily transportable to the point of use and converted into electricity wherever necessary [4,8,9]. However, in order to be economically competitive with the use of fossil fuels, low cost, stable and highly efficient semiconducting materials are required [10,11].

Among the many n-type semiconductors which have been extensively employed in the water oxidation half reaction, $BiVO_4$ is to date one of the best-performing metal oxide photoanode materials [10,12,13]. Thanks to its narrow band gap of *ca.* 2.4 eV in its monoclinic scheelite phase, it can absorb 9% of the solar spectrum, *i.e.* a larger fraction compared to the widely employed UV-absorber TiO_2 [9]. Furthermore, it is inexpensive and has a valence band (VB) which is far more positive than the water oxidation potential, providing sufficient overpotential for holes to oxidize water [12]. Despite these attractive features, $BiVO_4$ suffers from exceptionally small majority carrier mobility, insufficient charge separation and relatively slow injection of holes across the

semiconductor/electrolyte interface [12,14]. Moreover, since its conduction band (CB) edge located at 0.02 V *vs.* NHE [15] falls below the H^+ reduction potential, $BiVO_4$ is not able to produce H_2 from H_2O without an applied potential [16].

On the other hand, TiO_2, the most largely employed, stable and cost-effective photocatalyst, possesses a CB potential of -0.16 V *vs.* NHE (in the more photoactive anatase phase) [17], which is enough negative to reduce water. However, its relatively high energy band gap of 3.2 eV (anatase phase) makes it active only under UV light, which is only 3% of the solar spectrum incoming on the earth [18]. In this context, many strategies have been employed to make TiO_2 visible light-active [19–21], in particular through the insertion of dopant species [17,22,23], which may extend light absorption through the introduction of defective sites, and dye sensitization [24]. However, an excess of dopant impurities, acting as charge recombination centres, can have detrimental effects on TiO_2 photoefficiency [22], while organic dye sensitizers are known to undergo photodegradation over time [21].

Hence, the use of visible light responsive transition metal oxide semiconductors, which are stable under oxidative conditions, together with coupling different semiconductor materials in heterojunction systems [25,26], is an attractive strategy to extend the sensitivity of photocatalytic materials and improve their functionality. In fact, in these composite systems a more effective electron-hole separation may be achieved, which guarantees longer lifetime of the photogenerated charges and a generally enhanced photocatalytic performance with respect to the individual components [26,27].

For instance, coupling TiO_2 with WO_3 was demonstrated to limit the undesired recombination of photogenerated charge carriers, with the photoexcited electrons being

efficiently transferred from the TiO_2 to the WO_3 CB. However, this also results in an undesired decrease of their reducing power [28,29]. Moreover, Fe_2O_3 [30] and chalcogenide semiconductors, such as CdSe [31], characterized by smaller band gaps compared to TiO_2, were employed as sensitizers of transparent oxides to extend their photoactivity in the visible region. However, similarly to WO_3, Fe_2O_3 is not a good candidate to preserve the potential of TiO_2 for overall water splitting due to its too low CB edge energy [32], while chalcogenide materials, though having an ideal CB position for H_2 generation [10], are unsuitable because of their instability in water oxidation conditions.

In this frame $BiVO_4$, with its narrower band gap and good stability, emerges as a promising candidate to broaden the photoactivity of TiO_2 possibly without significant loss of reducing ability [14], since the $BiVO_4$ CB edge is located only *ca.* 0.2 eV below that of TiO_2 [15]. By coupling titanium dioxide with bismuth vanadate in the TiO_2/$BiVO_4$ heterojunction visible light sensitized TiO_2 can be obtained, which, thanks to its high reduction potential, can be employed for up-hill processes, such as water splitting into H_2 and O_2, under visible light irradiation [33]. In such a system, the excellent visible light harvesting properties of $BiVO_4$ may be combined with the TiO_2 CB potential suitable for proton reduction. However, on the basis of the relative band edge positions of pure TiO_2 and $BiVO_4$, a Type I band scheme [25] should be predicted for this heterojunction system which, under visible light irradiation, would result in the accumulation of photogenerated electrons and holes on the $BiVO_4$ side. Even though electron injection from the low-lying CB of $BiVO_4$ to the more negative CB of TiO_2 is in principle thermodynamically unfavoured, evidence that this may occur has been recently reported [34–44] and ascribed either to the presence of a Type II instead of the predicted Type I band alignment

[35,36,38,40,42–44], or to an unidentified defect-mediated charge transport pathway [34]. Moreover, evidence was provided for transfer into TiO_2 of high-energy electrons visible light excited in $BiVO_4$, with an unexpected activity in PEC water oxidation and photocatalytic production of H_2 [37].

Inspired by this intriguing phenomenon, in this work we investigated the $TiO_2/BiVO_4$ heterojunction trying to shed light on the mechanism through which high-energy electrons photoexcited in $BiVO_4$ under visible irradiation transfer into more reductive TiO_2. Optically transparent films of the composite system and of the pure components, for comparison, were prepared by spin coating deposition of precursor solutions through a low-cost and time saving process. Optically transparent photoelectrodes can be exploited in dual absorber tandem cells, in which two or more absorbing materials are sequentially stacked to maximize light absorption in the overall device [9]. The combination of PEC characterization and methyl viologen photocatalytic reduction tests provides evidence that highly reducing electrons, photopromoted in $BiVO_4$ under visible light irradiation, may transfer to TiO_2. The so realized heterojunction might in principle act as a stand-alone composite photoanode able to carry out complete solar water splitting.

2. Experimental

2.1. Chemicals and materials

The following chemicals, purchased from Sigma Aldrich, were employed as supplied: titanium diisopropoxide bis(acetylacetonate) (TIPA), 75 wt% in isopropanol, ammonium metavanadate, bismuth(III) nitrate pentahydrate (98%), poly(vinyl alcohol) >99%, citric acid (99%), glacial acetic acid, sodium sulfate, methyl viologen (MV^{2+}), nitric acid 23.3%,

isopropanol and ethanol (99%). Anhydrous sodium sulfite was purchased from Alfa Aesar; fluorine-doped tin oxide (FTO) glass, 2 mm thick, was purchased from Pilkington Glass (TEC-7).

2.2. Photoelectrode preparation

Titanium dioxide films were prepared under nitrogen atmosphere inside a glove box, starting with 1:3 dilution of TIPA with isopropanol, followed by spin coating the so obtained solution onto FTO at 2000 rpm for 30 s. Prior to deposition, the FTO glass was cleaned by 30 min-long sonication in a soap solution, then washed carefully, sonicated in ethanol for 30 min and dried in air. After coating, the film was dried for 1 h at 70 °C and then annealed for 1 h at 500 °C.

Bismuth vanadate films were prepared as reported elsewhere [15]. In a typical synthesis, 0.002 mol of $Bi(NO_3)_3$ and NH_4VO_3 were dissolved into 6 mL of 23.3% HNO_3 containing 0.004 mol of citric acid acting as a stabilizer. After complete dissolution of the precursors, 0.04 g of poly(vinyl alcohol) and 0.25 mL of acetic acid were added to 1.0 mL of the above solution to obtain a denser paste. A $BiVO_4$ layer was obtained by spin coating the paste at 4000 rpm for 30 s onto clean FTO, previously treated with acetone. The so obtained films were then annealed in air for 1 h at 70 °C and calcined in air for 1 h at 500 °C.

The $TiO_2/BiVO_4$ films were obtained by coating a TiO_2 electrode prepared as described above with the $BiVO_4$ dense paste. Then the composite film underwent the same thermal treatment used for single $BiVO_4$ films. An inverse $BiVO_4/TiO_2$ heterojunction photoanode was also prepared by covering a FTO/$BiVO_4$ electrode with a TiO_2 film, followed by thermal treatment.

The FTO/WO_3/$BiVO_4$ and CdS electrodes employed in MV^{2+} photocatalytic reduction tests were prepared through spin coating and chemical bath deposition [45,46], respectively.

2.3. Optical, structural and photoelectrochemical tests

UV−visible absorption spectra were recorded using a Jasco V-670 spectrophotometer. The crystalline phase of the materials was determined through X-ray powder diffraction (XRPD) analysis using a Philips PW1820 with Cu Kα radiation at 40 mA and 40 kV. Images showing the morphology and the cross section of the electrodes were obtained using a scanning electron microscope (SEM, model LEO 1430, Zeiss) operating at a 10 kV accelerating voltage, at a 8 mm working distance.

PEC measurements were carried out using a three electrode cell with an Ag/AgCl (3.0 M NaCl) reference electrode, a platinum gauze as a counter electrode and a Princeton Applied Research 2263 (PARstat) potentiostat. The photoanodes were tested under back side illumination (*i.e.,* through the FTO/TiO_2, FTO/$BiVO_4$ or FTO/TiO_2/$BiVO_4$ interface), in contact with a 0.5 M Na_2SO_3 aqueous solution buffered at pH 7 with a 0.5 M potassium phosphate buffer (KPi), acting as hole scavenger. The light source was an Oriel solar simulator (Model 81172) providing AM 1.5 G simulated solar illumination with 100 mW cm^{-2} intensity (1 sun). All semiconductor oxides are stable at neutral pH and no noticeable degradation was observed under irradiation. The potential *vs.* Ag/AgCl was converted into the RHE scale using the following equation: $E_{RHE} = E_{AgCl} + 0.059\ pH + E^o_{AgCl}$, with E^o_{AgCl} (3.0 M NaCl) = 0.210 V at 25 °C. All RHE values refer to pH = 0, *i.e.* they coincide with SHE values [47]. The linear sweep voltammetry (LSV) scan of each material was recorded

at 10 mV s^{-1} starting from the open circuit potential after 5 min irradiation, up to 0.7 V *vs.* Ag/AgCl, in order to avoid the electrochemical oxidation of sulfite.

The incident photon to current efficiency (IPCE) was measured both in 0.5 M aqueous Na_2SO_3 buffered at pH 7 with 0.5 M KPi and in 0.5 M aqueous Na_2SO_4, using the same single-compartment three-electrode cell. The IPCE was calculated using the following equation:

$$IPCE = \frac{[1240 \times J]}{P_\lambda \times \lambda} \times 100$$

where J is the photocurrent density (mA cm^{-2}) and P_λ (mW cm^{-2}) is the power of the monochromatic light at wavelength λ (nm).

2.4. Methyl viologen photocatalytic reduction tests

A 25×8 mm^2 film was placed in a 100 mm thick vacuum cuvette containing 3 mL of 1.0 mM MV^{2+} solution in ethanol. The light source was a 200 W Xe lamp equipped with a water filter (Lot Oriel) and a 420 nm cutoff filter (Thorlabs), in order to cut the IR and the UV portion of the emission spectrum and obtain visible irradiation with 30 mW cm^{-2} power intensity. By this way MV^{2+} self-reduction, occurring under irradiation with wavelength up to 390 nm, and the direct excitation of TiO_2 were both excluded. The light power intensity was checked using a Thorlabs PM200 power meter equipped with a S130VC power head with a Si detector. Before each experiment, the vacuum cuvette was filled with the MV^{2+} ethanol solution in a N_2 purged glove box, in order to remove any trace of O_2, possibly acting as undesired electron acceptor during the photoreduction experiment. The same film area was irradiated in all experiments, by selecting it through a mask. The increase in concentration of the reduced methyl viologen ($MV^{+\cdot}$) species was monitored during the

experiment by recording, at selected time intervals, the absorption spectrum of the solution, which assumes an increasing blue color under irradiation.

3. Results and discussion

3.1. Photoelectrodes characterization

The X-ray powder diffraction patterns of the TiO_2, $BiVO_4$ and $BiVO_4/TiO_2$ electrodes are reported in Fig. 1a. The pattern observed for $BiVO_4$ fits well with that relative to the monoclinic structure, while the characteristic (101) reflection of TiO_2 anatase at $2\theta = 25.5°$ is evident in both the individual TiO_2 film and the composite material, as shown in the inset of Fig. 1a. Other reflections typical of anatase cannot be appreciated due to their lower intensity and to the overlap of some of them with more intense signals originated from FTO. The XRPD spectrum obtained with the combined $BiVO_4/TiO_2$ material, i.e. with TiO_2 as top layer, exhibits the reflection patterns of both components, indicating that no other phase was formed upon coupling the two oxides.

The absorption spectra of pure TiO_2 and $BiVO_4$ films and of both $TiO_2/BiVO_4$ and $BiVO_4/TiO_2$ heterojunctions are reported in Fig. 1b. The TiO_2 thin film is transparent in the visible range; its absorption onset, at *ca.* 400 nm as expected from the 3.2 eV band gap of TiO_2 anatase, overlaps with interference fringes. The $BiVO_4$ photoanode (band gap of 2.4 eV) absorbs in the visible range up to *ca.* 500 nm. Lower absorption is obtained in this region when $BiVO_4$ is coupled with TiO_2 in both $TiO_2/BiVO_4$ and $BiVO_4/TiO_2$ heterojunctions, as shown in Fig. 1b. This unexpected phenomenon, in which a colored film loses absorption when covered with a transparent layer, may find an explanation in electronic structure effects consequent with the equilibration of the Fermi levels of the two

oxides. Furthermore, the absorption onset of both coupled systems is seemingly shifted to higher energy values with respect to that of individual $BiVO_4$, which might also be related to Fermi levels equilibration effects at the heterojunction.

The top view SEM images of the $BiVO_4$ and $TiO_2/BiVO_4$ heterojunction films are reported in Fig. 2. They show an aggregated network of particles, with the $BiVO_4$ film (Fig. 2a) characterized by a worm-like shape morphology similar to that obtained in previous studies [15,45], and by a discontinuous coating of the FTO underlayer. Differently, in the $TiO_2/BiVO_4$ heterojunction film (Fig. 2b) the FTO asperities are completely covered by the TiO_2 and $BiVO_4$ layers. Moreover, the $BiVO_4$ top layer in the composite system appears as a compact film, which completely covers the TiO_2 layer due to the different affinity of $BiVO_4$ for TiO_2 rather than for FTO.

From the cross section SEM images shown in Fig. 3 a thickness of *ca.* 55, 60 and 100 nm was calculated for the $BiVO_4$, TiO_2, and overall $TiO_2/BiVO_4$ layers, respectively, by subtracting the average thickness of FTO (546 nm, obtained from Fig. 3a) from the average thickness of the $FTO/BiVO_4$, FTO/TiO_2 and $FTO/TiO_2/BiVO_4$ systems (Fig. 3b, c and d, respectively). The so calculated thickness of the bare $BiVO_4$ film is in accordance with that obtained for $BiVO_4$ films prepared by the same procedure [15]. Furthermore, the thickness of the $TiO_2/BiVO_4$ heterojunction system is in line with the thickness of the single component layers.

3.2. Photoelectrochemical performance of the electrodes

The PEC performance of the investigated $TiO_2/BiVO_4$ heterojunction as photoanode material was compared with that of single TiO_2 in contact with a Na_2SO_3 solution at pH 7

(0.5 M KPi). In the presence of this hole scavenger the performance of the heterojunction electrode is not affected by the typically slow water oxidation kinetics at the $BiVO_4$ surface [35]. As PEC experiments were performed by irradiating the photoanodes through the FTO/oxide film interface, in the composite material visible light first passed through the TiO_2 film and promoted electrons in $BiVO_4$, close to the interface between the two semiconductors. Thus the mobility of the electrons photopromoted in the CB of $BiVO_4$ was not affected by its poor electron transport properties [48,49].

The LSV plots recorded with the TiO_2 and the $TiO_2/BiVO_4$ photoanodes, under both full lamp solar simulated irradiation and visible light irradiation at $\lambda > 420$ nm, are shown in Fig. 4a. Under full lamp irradiation the TiO_2 photoanode produced a relatively small photocurrent, as expected from its limited ability to absorb solar radiation (see Fig. 1b), and no appreciable photocurrent was produced under visible light irradiation, as expected. Under full lamp irradiation, *i.e.* under conditions of simultaneous excitation of both semiconductor oxides, the photocurrent produced at 1.0 V *vs.* RHE by the $TiO_2/BiVO_4$ heterojunction photoanode was 10-fold higher than that produced by the TiO_2 photoanode, thanks to the ability of $BiVO_4$ in absorbing a larger part of the solar spectrum. The combined photoanode thus exhibits considerable photoactivity even under visible light excitation ($\lambda > 420$ nm), which can be absorbed by $BiVO_4$ only.

Since the procedure here adopted for the preparation of TiO_2 films even in the composite system ensures the formation of compact and pin hole-free TiO_2 layers [50], electrons visible light excited in $BiVO_4$ can flow to the FTO glass only through the TiO_2 film. Therefore, due to the *ca.* 0.2 eV energy mismatch between the CB of TiO_2 and

$BiVO_4$, only the electrons with an energy excess with respect to the CB edge of $BiVO_4$ (0.02 V *vs.* RHE at pH 0 [15]) are able to transfer to the more negative CB of anatase TiO_2 (–0.16 V *vs.* RHE at pH 0 [17]). For this reason a relatively lower photocurrent density value is expected with the $TiO_2/BiVO_4$ heterojunction compared to pure $BiVO_4$ photoanodes [40].

The LSV analyses reported in Fig. 4a also show that the TiO_2 photoanode exhibits a much more negative photocurrent onset with respect to that found for the $TiO_2/BiVO_4$ heterojunction. The photocurrent onsets measured by this way provide a good indication of the flat band potential (V_{FB}) of the material [15,51]. In order to ascertain the V_{FB} position of the investigated heterojunction with respect to those of the two individual components, we recorded their open circuit potentials (OCP) under 5 min long solar simulated irradiation (1 sun) [52], in contact with the Na_2SO_3 electrolyte solution. We obtained OCP values of 0.003 V, 0.203 V and 0.253 V *vs.* RHE (pH 0) for the TiO_2, $TiO_2/BiVO_4$ heterojunction and $BiVO_4$ electrode, respectively, with the heterojunction OCP value in line with the CB edge alignment which follows the equilibration of the Fermi levels of the two oxides in the heterojunction.

The IPCE plots reported in Fig. 4b evidence that TiO_2 is active only up to 410 nm, consistently with its 3.2 eV band gap, while it becomes photoactive under visible light irradiation when coupled with $BiVO_4$, acting as visible light sensitizer up to 490 nm. Since $BiVO_4$ alone is photoactive up to 520 nm [15], the energy difference between the photocurrent onsets of pure $BiVO_4$ and of the $TiO_2/BiVO_4$ heterojunction composite system should correspond to the extra energy required for visible light excited electrons in $BiVO_4$ to be injected into the TiO_2 CB.

The IPCE in water splitting measured at 1.23 V *vs.* RHE with the electrodes in contact with a Na_2SO_4 aqueous solution are shown in Fig. 5. The null conversion efficiency of TiO_2 in the visible region is confirmed. The lower photoactivity of the two $BiVO_4$-containing colored materials compared to those obtained in contact with the Na_2SO_3 solution should be ascribed to the slow water oxidation kinetics typical of $BiVO_4$, in the absence of any hole scavenger or co-catalyst for oxygen evolution [53,54]. The visible light sensitizer role of $BiVO_4$ in the composite system is evident also in this case. Furthermore, under such unfavorable oxidation kinetics conditions, the IPCE values obtained with the $TiO_2/BiVO_4$ heterojunction up to *ca.* 480 nm are higher not only than those obtained with TiO_2, but also compared to those obtained with single $BiVO_4$, suggesting that partial charge separation occurs in the composite system.

3.3. Photocatalytic methyl viologen reduction tests

Photocatalytic methyl viologen reduction tests were performed to investigate the photocatalytic reduction ability of the $TiO_2/BiVO_4$ heterojunction in comparison with those of other commonly employed semiconductors [55–58]. The mono-electron reduction of the almost colorless MV^{2+} to the blue $MV^{+\cdot}$ reduced form (Fig. 6), occurring at –0.03 V *vs.* NHE [59,60], was monitored by measuring the absorption of a 1.0 mM solution of MV^{2+} in ethanol under visible light irradiation ($\lambda > 420$ nm). Such irradiation conditions prevent MV^{2+} self-reduction, occurring under UV irradiation and, in the case of the $TiO_2/BiVO_4$ electrode, exclude the direct excitation of TiO_2 which, due to its negative CB potential, would very efficiently induce MV^{2+} reduction.

The experiment was carried out with the tested film initially in contact with the MV^{2+} solution under nitrogen atmosphere, in order to avoid the reversible oxidation of the $MV^{+\cdot}$ species in the presence of oxygen [55]. In addition to the investigated $TiO_2/BiVO_4$ heterojunction, other common semiconductors with known CB potential location were tested for comparison, *i.e.* the pure TiO_2 and $BiVO_4$ components having a CB potential edge at *ca.* –0.16 V (in the anatase phase) [17] and 0.02 V [15] *vs.* NHE, respectively, the $WO_3/BiVO_4$ heterojunction, known for its excellent charge separation properties [61], with a CB edge at *ca.* 0.19 V *vs.* NHE [15], and CdS, characterized by extended absorption in the visible up to *ca.* 550 nm [62] and by a highly negative CB potential of *ca.* –0.4 V *vs.* NHE [63], *i.e.* significantly more negative than the reduction potential of the $MV^{2+}/MV^{+\cdot}$ couple. The photocatalytic reduction efficiency of all investigated materials was tested under 2-h long irradiation, up to the attainment of a plateau.

The absorption spectra of the probe solution recorded at different time during the photoreduction experiment in the presence of the $TiO_2/BiVO_4$ heterojunction and of the pure $BiVO_4$ are shown in Fig. 7a and 7b, respectively. The formation of the blue reduced $MV^{+\cdot}$ species was testified by the absorbance increase over time, which clearly occurred at a higher rate when the experiment was carried out with the $TiO_2/BiVO_4$ coupled system. Thus, the composite material is clearly more efficient than pure $BiVO_4$ in MV^{2+} reduction.

Fig. 7c reports the $MV^{+\cdot}$ maximum absorbance at 606 nm *vs.* the irradiation time plots for all tested semiconductor materials, providing information on their relative photocatalytic reduction efficiency under visible light irradiation. As expected, TiO_2 shows negligible photoactivity. Indeed, despite its highly negative CB potential, its poor visible light absorption ability limits its activity under the here employed irradiation conditions, in

line with the IPCE results shown in Fig. 4b and 5. Also the $WO_3/BiVO_4$ heterojunction shows little photoactivity despite it absorbs light up to *ca.* 500 nm and possesses excellent charge separation properties [15,45]. The limiting factor should thus be identified in this case with the much more positive CB edge position (0.19 V *vs.* NHE) of the $WO_3/BiVO_4$ heterojunction with respect to the reduction potential of MV^{2+}. Furthermore, the $WO_3/BiVO_4$ heterojunction shows lower ability in MV^{2+} reduction than individual $BiVO_4$ (Fig. 7c), supporting a downward $BiVO_4$ flat band equilibration when the $WO_3/BiVO_4$ heterojunction is formed [15]. This rules out the hypothesis that the improved charge separation typical of heterojunction systems is sufficient to explain the higher photocatalytic activity in MV^{2+} reduction obtained with the $TiO_2/BiVO_4$ heterojunction compared to the single components. Indeed, Fig. 7c shows that after 1 h-long visible light irradiation, the $MV^{+\cdot}$ concentration attained in contact with the $TiO_2/BiVO_4$ heterojunction is 10- and 3-fold higher than in contact with the TiO_2 and $BiVO_4$ films, respectively. The $TiO_2/BiVO_4$ heterojunction exhibits high MV^{2+} reduction ability, which is lower only to that of CdS, having a CB potential significantly more negative than the reduction potential of the $MV^{2+}/MV^{+\cdot}$ couple. This demonstrates that under visible light irradiation highly reducing electrons are produced in the $TiO_2/BiVO_4$ heterojunction, at a more negative potential than those visible light promoted in single $BiVO_4$.

As expected, the highest photoreduction efficiency was attained with the semiconductor systems having the most negative CB edge value. Therefore, by comparing the photocatalytic tests results with the CB edge position values reported in the literature, the apparent relative scale shown in Fig. 7d can be drawn for the CB edge energy of the tested materials, with respect to the reduction potential of the $MV^{2+}/MV^{+\cdot}$ couple. Thus, only CdS

and TiO_2 have a CB edge potential negative enough to efficiently photoreduce MV^{2+}. $BiVO_4$, although having a slightly more positive CB potential, is still able to photoreduce MV^{2+}, thanks to electrons photoexcited above the CB edge having higher energy compared to the $MV^{2+}/MV^{+\cdot}$ couple reduction potential. On the other hand, the CB potential of the $WO_3/BiVO_4$ heterojunction is more positive than that of $BiVO_4$ and this results in a low MV^{2+} reduction efficiency.

3.4. Proposed mechanism

High-energy electron injection, active under visible light excitation, from the CB of $BiVO_4$ to the more negative CB of TiO_2 is required to explain the unexpected PEC performance as well as the visible light photocatalytic activity in MV^{2+} reduction of the $TiO_2/BiVO_4$ heterojunction. A schematic representation, based on the band edge positions of the two isolated semiconductors [15,17] and their band gap values, is shown in Fig. 8. PEC analysis of the $TiO_2/BiVO_4$ heterojunction under visible light irradiation ($\lambda > 420$ nm) demonstrates that photopromoted electrons resulting from the selective excitation of the $BiVO_4$ layer and having enough energy above the $BiVO_4$ CB bottom to reach the same energy level as the TiO_2 CB bottom, can effectively transfer to TiO_2. The required energy excess can be quantified on the basis of the results of the IPCE analyses shown in Figs. 4b and 5, and it should be around 0.2 eV, *i.e.* the energy difference associated with the photocurrent onset of the $TiO_2/BiVO_4$ and $BiVO_4$ electrodes (490 and 520 nm, respectively). Therefore, if the transfer of these electrons from $BiVO_4$ to TiO_2 occurs efficiently, and an intimate contact between the two semiconductors is crucial to this aim, the charge couples photogenerated in $BiVO_4$ under visible light irradiation can be

efficiently separated at the opposite sides of the heterojunction, with beneficial effects on photoactivity.

On the other hand, methyl viologen photocatalytic reduction tests in the absence of any external bias imply that the electron transfer towards the probe solution is mainly driven by the energy difference between the CB edge position of each photocatalyst system and the reduction potential of MV^{2+}. Therefore, the higher efficiency of the $TiO_2/BiVO_4$ heterojunction with respect to pure $BiVO_4$ may only be ascribed to the actual involvement of visible light photopromoted, highly reducing electrons. On the basis of the Fermi level equilibration between the TiO_2 and $BiVO_4$ components, the consequent shift towards a more negative value of the flat band potential at the heterojunction with respect to pure $BiVO_4$ (as confirmed by OCP values, see Section 3.2.) contributes in increasing the reductive power of photopromoted electrons in the $TiO_2/BiVO_4$ coupled system. In fact, the highly reducing electrons lying in the so obtained $TiO_2/BiVO_4$ CB should be more prone than those in $BiVO_4$ CB to reduce MV^{2+}, with a consequent beneficial effect on the overall efficiency of the investigated process.

4. Conclusions

The $TiO_2/BiVO_4$ heterojunction is a fascinating material which allows to exploit the excellent absorption properties of $BiVO_4$ to produce highly reductive electrons through TiO_2 sensitization under visible light. A counterintuitive electron transfer mechanism is active in this system, which significantly deviates from predictions based on the CB edges of the two isolate semiconductors. Methyl viologen reduction tests demonstrate the higher photocatalytic activity under visible light of the $TiO_2/BiVO_4$ heterojunction with respect to

either individual components and also compared to the $WO_3/BiVO_4$ heterojunction, which is characterized by excellent charge separation but is affected by a lower reducing ability than individual $BiVO_4$. The $TiO_2/BiVO_4$ heterojunction system allows TiO_2 sensitization for solar energy storage applications and has the potential to carry out overall water splitting under visible light, even without the application of an external bias.

Acknowledgments

The present work received support from the Cariplo Foundation project entitled *Novel Photocatalytic Materials Based on Heterojunctions for Solar Energy Conversion* (Fondazione Cariplo grant 2013-0615) and from the MIUR PRIN 2015K7FZLH project. The use of instrumentation purchased through the Regione Lombardia-Fondazione Cariplo joint *SmartMatLab* project (Fondazione Cariplo grant 2013-1766) is also acknowledged.

References

[1] M.G. Walter, E.L. Warren, J.R. McKone, S.W. Boettcher, Q. Mi, E.A. Santori, N.S. Lewis, Chem. Rev. 110 (2010) 6446–6473.

[2] Y. Tachibana, L. Vayssieres, J.R. Durrant, Nat. Photonics 6 (2012) 511–518.

[3] N.S. Lewis, D.G. Nocera, Proc. Natl. Acad. Sci. 103 (2006) 15729–15735.

[4] T. Hisatomi, J. Kubota, K. Domen, Chem. Soc. Rev. 43 (2014) 7520–7535.

[5] a Fujishima, K. Honda, Nature 238 (1972) 37–38.

[6] J. Brillet, J.-H. Yum, M. Cornuz, T. Hisatomi, R. Solarska, J. Augustynski, M. Graetzel, K. Sivula, Nat. Photonics 6 (2012) 824–828.

[7] H. Yi, D. Huang, L. Qin, G. Zeng, C. Lai, M. Cheng, S. Ye, B. Song, X. Ren, X. Guo, Appl. Catal. B Environ. 239 (2018) 408–424.

[8] K. Sivula, J. Phys. Chem. Lett. 4 (2013) 1624–1633.

[9] M.S. Prévot, K. Sivula, J. Phys. Chem. C 117 (2013) 17879–17893.

[10] K. Sivula, R. van de Krol, Nat. Rev. Mater. 1 (2016) 15010.

[11] Y. Yang, C. Zhang, C. Lai, G. Zeng, D. Huang, M. Cheng, J. Wang, F. Chen, C. Zhou, W. Xiong, Adv. Colloid Interface Sci. 254 (2018) 76–93.

[12] Y. Park, K.J. McDonald, K.-S. Choi, Chem. Soc. Rev. 42 (2013) 2321–2337.

[13] A. Kudo, K. Ueda, H. Kato, I. Mikami, Catal. Letters 53 (1998) 229–230.

[14] F.F. Abdi, R. van de Krol, J. Phys. Chem. C 116 (2012) 9398–9404.

[15] I. Grigioni, K.G. Stamplecoskie, E. Selli, P. V. Kamat, J. Phys. Chem. C 119 (2015) 20792–20800.

[16] S.P. Berglund, D.W. Flaherty, N.T. Hahn, A.J. Bard, C.B. Mullins, J. Phys. Chem. C 115 (2011) 3794–3802.

[17] M.V. Dozzi, B. Ohtani, E. Selli, Phys. Chem. Chem. Phys. 13 (2011) 18217.

[18] S.T. Kochuveedu, D.-P. Kim, D.H. Kim, J. Phys. Chem. C 116 (2012) 2500–2506.

[19] J. Schneider, M. Matsuoka, M. Takeuchi, J. Zhang, Y. Horiuchi, M. Anpo, D.W. Bahnemann, Chem. Rev. 114 (2014) 9919–9986.

[20] H. Park, Y. Park, W. Kim, W. Choi, J. Photochem. Photobiol. C Photochem. Rev. 15 (2013) 1–20.

[21] M. Pelaez, N.T. Nolan, S.C. Pillai, M.K. Seery, P. Falaras, A.G. Kontos, P.S.M. Dunlop, J.W.J. Hamilton, J.A. Byrne, K. O'Shea, M.H. Entezari, D.D. Dionysiou, Appl. Catal. B Environ. 125 (2012) 331–349.

[22] M.V. Dozzi, E. Selli, J. Photochem. Photobiol. C Photochem. Rev. 14 (2013) 13–28.

[23] M.V. Dozzi, A. Candeo, G. Marra, C. D'Andrea, G. Valentini, E. Selli, J. Phys. Chem. C 122 (2018) 14326–14335.

[24] S. Zheng, Z. Wei, K. Yoshiiri, M. Braumüller, B. Ohtani, S. Rau, E. Kowalska, Photochem. Photobiol. Sci. 15 (2016) 69–79.

[25] S.J.A. Moniz, S.A. Shevlin, D.J. Martin, Z.-X. Guo, J. Tang, Energy Environ. Sci. 8 (2015) 731–759.

[26] H. Wang, L. Zhang, Z. Chen, J. Hu, S. Li, Z. Wang, J. Liu, X. Wang, Chem. Soc. Rev. 43 (2014) 5234.

[27] I. Grigioni, K.G. Stamplecoskie, D.H. Jara, M.V. Dozzi, A. Oriana, G. Cerullo, P. V. Kamat, E. Selli, ACS Energy Lett. 2 (2017) 1362–1367.

[28] M.V. Dozzi, S. Marzorati, M. Longhi, M. Coduri, L. Artiglia, E. Selli, Appl. Catal. B Environ. 186 (2016) 157–165.

[29] F. Riboni, M.V. Dozzi, M.C. Paganini, E. Giamello, E. Selli, Catal. Today 287 (2017) 176–181.

[30] P. Luan, M. Xie, D. Liu, X. Fu, L. Jing, Sci. Rep. 4 (2014) 4–10.

[31] J.H. Bang, P. V. Kamat, Adv. Funct. Mater. 20 (2010) 1970–1976.

[32] K. Sivula, F. Le Formal, M. Grätzel, ChemSusChem 4 (2011) 432–449.

[33] A. Kudo, Catal. Surv. from Asia 7 (2003) 31–38.

[34] X. An, T. Li, B. Wen, J. Tang, Z. Hu, L.-M. Liu, J. Qu, C.P. Huang, H. Liu, Adv. Energy Mater. 6 (2016) 1502268.

[35] L.H. Hess, J.K. Cooper, A. Loiudice, C.-M. Jiang, R. Buonsanti, I.D. Sharp, Nano Energy 34 (2017) 375–384.

[36] H. Li, H. Yu, X. Quan, S. Chen, H. Zhao, Adv. Funct. Mater. 25 (2015) 3074–3080.

[37] M. Xie, X. Fu, L. Jing, P. Luan, Y. Feng, H. Fu, Adv. Energy Mater. 4 (2014) 1300995.

[38] H. Zhang, C. Cheng, ACS Energy Lett. 2 (2017) 813–821.

[39] A.P. Singh, N. Kodan, B.R. Mehta, A. Held, L. Mayrhofer, M. Moseler, ACS Catal. 6 (2016) 5311–5318.

[40] B.-Y. Cheng, J.-S. Yang, H.-W. Cho, J.-J. Wu, ACS Appl. Mater. Interfaces 8 (2016) 20032–20039.

[41] L. Zhang, G. Tan, S. Wei, H. Ren, A. Xia, Y. Luo, Ceram. Int. 39 (2013) 8597–8604.

[42] Y. Hu, D. Li, Y. Zheng, W. Chen, Y. He, Y. Shao, X. Fu, G. Xiao, Appl. Catal. B Environ. 104 (2011) 30–36.

[43] J. Resasco, H. Zhang, N. Kornienko, N. Becknell, H. Lee, J. Guo, A.L. Briseno, P. Yang, ACS Cent. Sci. 2 (2016) 80–88.

[44] S. Ho-Kimura, S.J.A. Moniz, A.D. Handoko, J. Tang, J. Mater. Chem. A 2 (2014) 3948.

[45] I. Grigioni, A. Corti, M.V. Dozzi, E. Selli, J. Phys. Chem. C 122 (2018) 13969–13978.

[46] C. Lu, L. Zhang, Y. Zhang, S. Liu, G. Liu, Appl. Surf. Sci. 319 (2014) 278–284.

[47] R.W. Ramette, J. Chem. Educ. 64 (1987) 885.

[48] Y. Liang, T. Tsubota, L.P.A. Mooij, R. van de Krol, J. Phys. Chem. C 115 (2011) 17594–17598.

[49] F.F. Abdi, T.J. Savenije, M.M. May, B. Dam, R. van de Krol, J. Phys. Chem. Lett. 4 (2013) 2752–2757.

[50] N. Chandrasekharan, P. V. Kamat, J. Phys. Chem. B 104 (2000) 10851–10857.

[51] J.A. Turner, J. Chem. Educ. 60 (1983) 327.

[52] Z. Chen, T.F. Jaramillo, T.G. Deutsch, A. Kleiman-Shwarsctein, A.J. Forman, N. Gaillard, R. Garland, K. Takanabe, C. Heske, M. Sunkara, E.W. McFarland, K. Domen, E.L. Miller, J.A. Turner, H.N. Dinh, J. Mater. Res. 25 (2010) 3–16.

[53] L. Cai, J. Zhao, H. Li, J. Park, I.S. Cho, H.S. Han, X. Zheng, ACS Energy Lett. 1 (2016) 624–632.

[54] T.W. Kim, K.-S. Choi, Science (80-.). 343 (2014) 990–994.

[55] S. Ikeda, N. Sugiyama, S. Murakami, H. Kominami, Y. Kera, H. Noguchi, K. Uosaki, T. Torimoto, B. Ohtani, Phys. Chem. Chem. Phys. 5 (2003) 778–783.

[56] S. Krishnamurthy, I. V. Lightcap, P. V. Kamat, J. Photochem. Photobiol. A Chem. 221 (2011) 214–219.

[57] P.E. De Jongh, D. Vanmaekelbergh, J.J. Kelly, (1999) 1069–1070.

[58] K.G. Stamplecoskie, Y.-S. Chen, P. V. Kamat, J. Phys. Chem. C 118 (2014) 1370–1376.

[59] C.L. Bird, A.T. Kuhn, Chem. Soc. Rev. 10 (1981) 49.

[60] M.F. Finlayson, B.L. Wheeler, N. Kakuta, K.H. Park, A.J. Bard, A. Campion, M.A. Fox, S.E. Webber, J.M. White, J. Phys. Chem. 89 (1985) 5676–5681.

[61] I. Grigioni, M. Abdellah, A. Corti, M.V. Dozzi, L. Hammarström, E. Selli, J. Am. Chem. Soc. 140 (2018) 14042–14045.

[62] F.Q. Zhou, J.C. Fan, Q.J. Xu, Y.L. Min, Appl. Catal. B Environ. 201 (2017) 77–83.

[63] D. Robert, Catal. Today 122 (2007) 20–26.

Figure captions

Fig. 1. (a) X-ray powder diffraction patterns of the TiO_2, $BiVO_4$ and $BiVO_4/TiO_2$ heterojunction films, where ● refer to FTO, ■ to $BiVO_4$ and ▼ to anatase TiO_2 reflections. Inset: enlargement of the 24.0 – 27.5° 2θ range, with the characteristic (101) reflection of anatase TiO_2. (b) Absorption spectra of 1) $TiO_2/BiVO_4$ and 2) $BiVO_4/TiO_2$ heterojunctions, 3) $BiVO_4$ and 4) TiO_2.

Fig. 2. Top view SEM images of (a) $BiVO_4$ and (b) $TiO_2/BiVO_4$ heterojunction photoanodes. The scale bar is 500 nm.

Fig. 3. Cross section SEM images of (a) clean FTO, (b) $BiVO_4$, (c) TiO_2 and (d) $TiO_2/BiVO_4$ heterojunction photoanodes. The scale bar is 250 nm.

Fig. 4. (a) Linear sweep voltammetry (LSV) and (b) incident photon to current efficiency (IPCE) analyses at 1.0 V *vs.* RHE of TiO_2 and of the $TiO_2/BiVO_4$ heterojunction, in 0.5 M Na_2SO_3 buffered at pH = 7 with 0.5 M potassium phosphate.

Fig. 5. Incident photon to current efficiency (IPCE) analysis of TiO_2, $BiVO_4$ and of the $TiO_2/BiVO_4$ heterojunction at 1.23 V *vs.* RHE, in 0.5 M Na_2SO_4.

Fig. 6. Reduction reaction of methyl viologen (MV^{2+}) to its mono-electron reduced $MV^{+\cdot}$ form.

Fig. 7. Absorption spectra recorded during methyl viologen (MV^{2+}) photoreduction experiments in the presence of (a) the $TiO_2/BiVO_4$ heterojunction and (b) pure $BiVO_4$. (c) Kinetic profiles (maximum $MV^{+\cdot}$ absorbance at 606 nm *vs.* time plots) obtained with

different semiconductor systems in photocatalytic MV^{2+} reduction tests. (d) CB energy scale of the tested semiconductor systems compared to the $MV^{2+}/MV^{+\cdot}$ reduction potential. All potential values are taken from the literature: see refs. [63] for CdS, [17] for TiO_2, [59,60] for $MV^{2+}/MV^{+\cdot}$, [15] for $BiVO_4$ and the WO_3/ $BiVO_4$ heterojunction.

Fig. 8. Proposed electron injection mechanism for the $TiO_2/BiVO_4$ heterojunction under visible light irradiation.

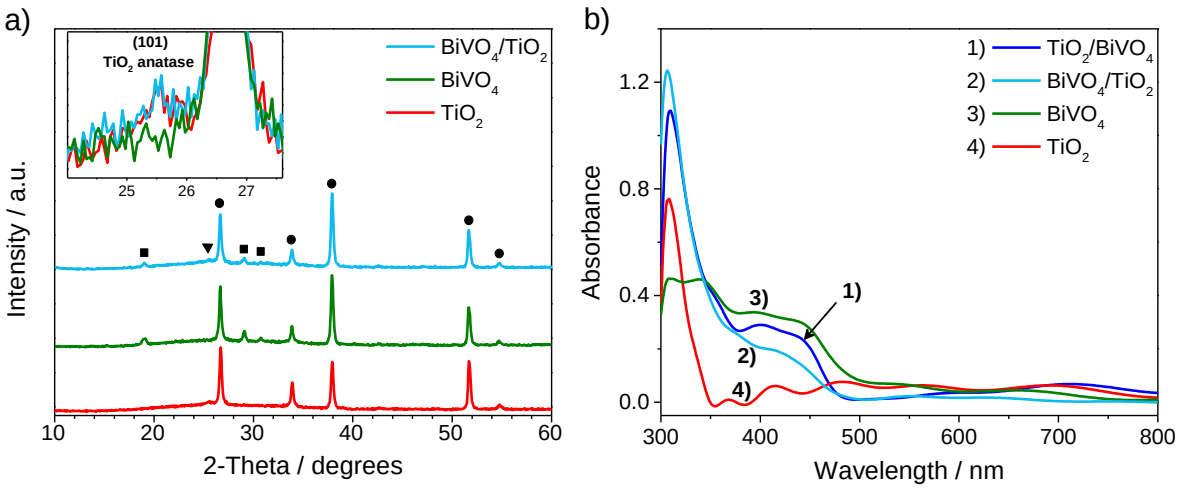

Fig. 1. (a) X-ray powder diffraction patterns of the TiO_2, $BiVO_4$ and $BiVO_4/TiO_2$ heterojunction films, where ● refer to FTO, ■ to $BiVO_4$ and ▼ to anatase TiO_2 reflections. Inset: enlargement of the 24.0 – 27.5° 2θ range, with the characteristic (101) reflection of anatase TiO_2. (b) Absorption spectra of 1) $TiO_2/BiVO_4$ and 2) $BiVO_4/TiO_2$ heterojunctions, 3) $BiVO_4$ and 4) TiO_2.

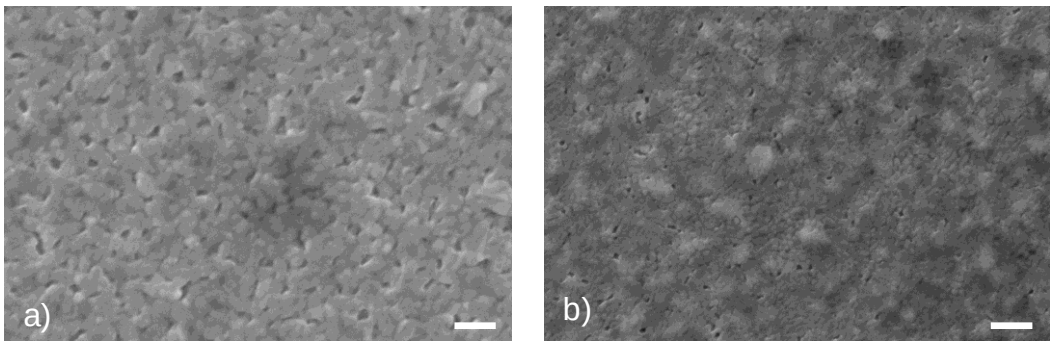

Fig. 2. Top view SEM images of (a) $BiVO_4$ and (b) $TiO_2/BiVO_4$ heterojunction photoanodes. The scale bar is 500 nm.

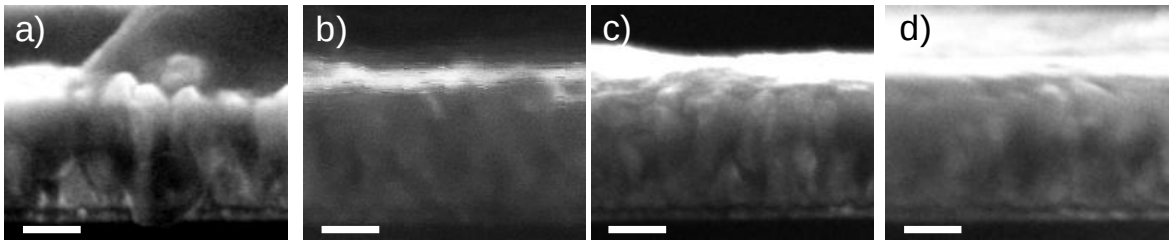

Fig. 3. Cross section SEM images of (a) clean FTO, (b) $BiVO_4$, (c) TiO_2 and (d) $TiO_2/BiVO_4$ heterojunction photoanodes. The scale bar is 250 nm.

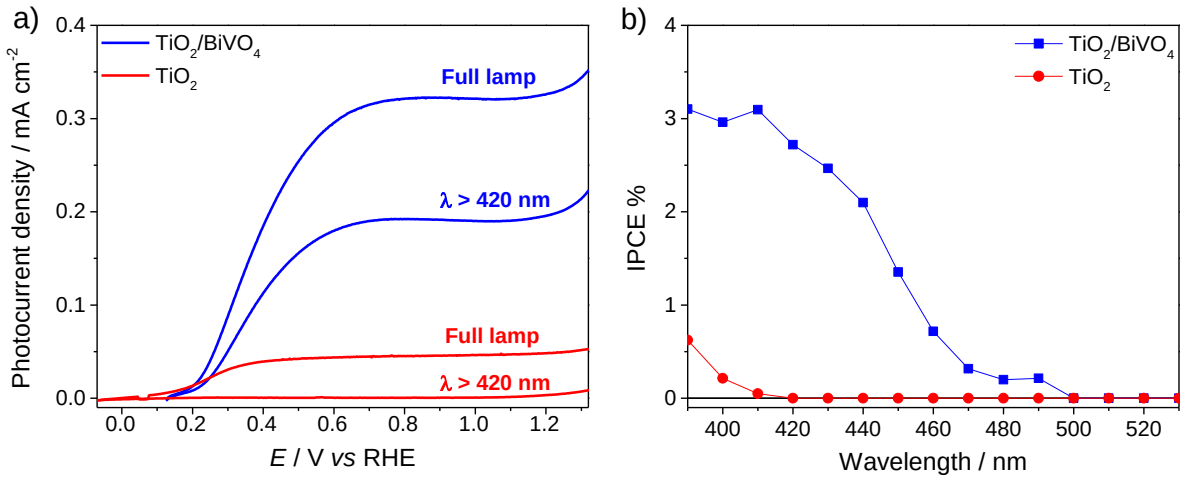

Fig. 4. (a) Linear sweep voltammetry (LSV) and (b) incident photon to current efficiency (IPCE) analyses at 1.0 V *vs.* RHE of TiO_2 and of the $TiO_2/BiVO_4$ heterojunction, in 0.5 M Na_2SO_3 buffered at pH = 7 with 0.5 M potassium phosphate.

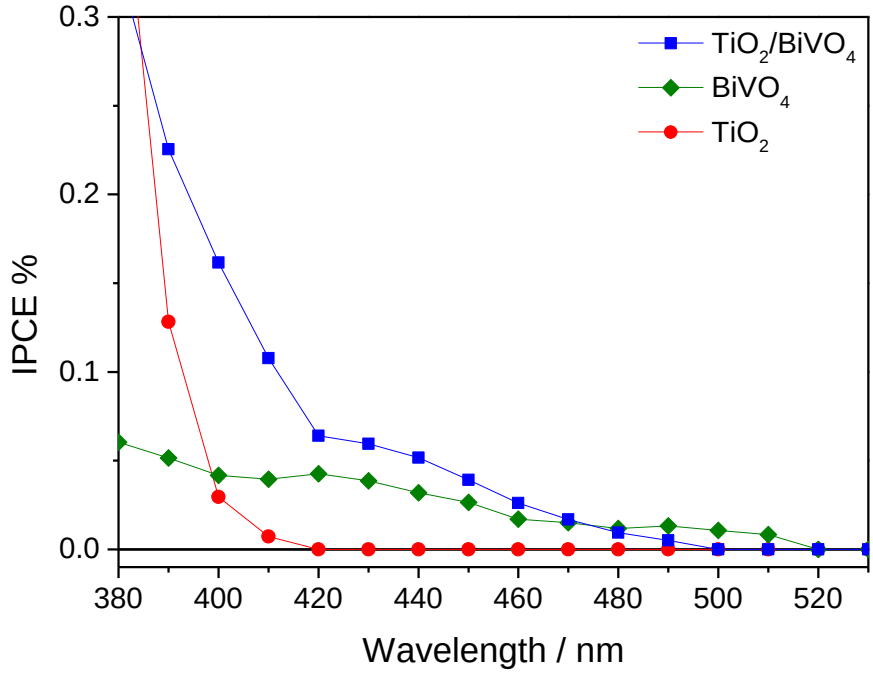

Fig. 5. Incident photon to current efficiency (IPCE) analysis of TiO_2, $BiVO_4$ and of the $TiO_2/BiVO_4$ heterojunction at 1.23 V *vs.* RHE, in 0.5 M Na_2SO_4.

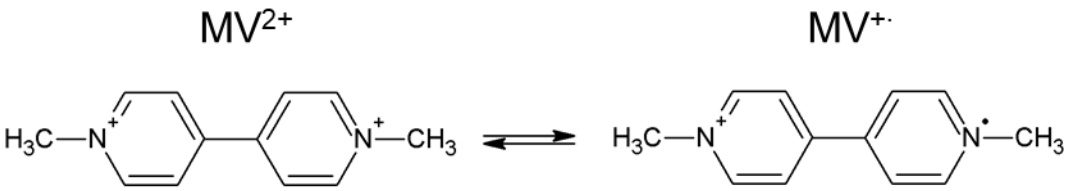

Fig. 6. Reduction reaction of methyl viologen (MV^{2+}) to its mono-electron reduced $MV^{+\cdot}$ form.

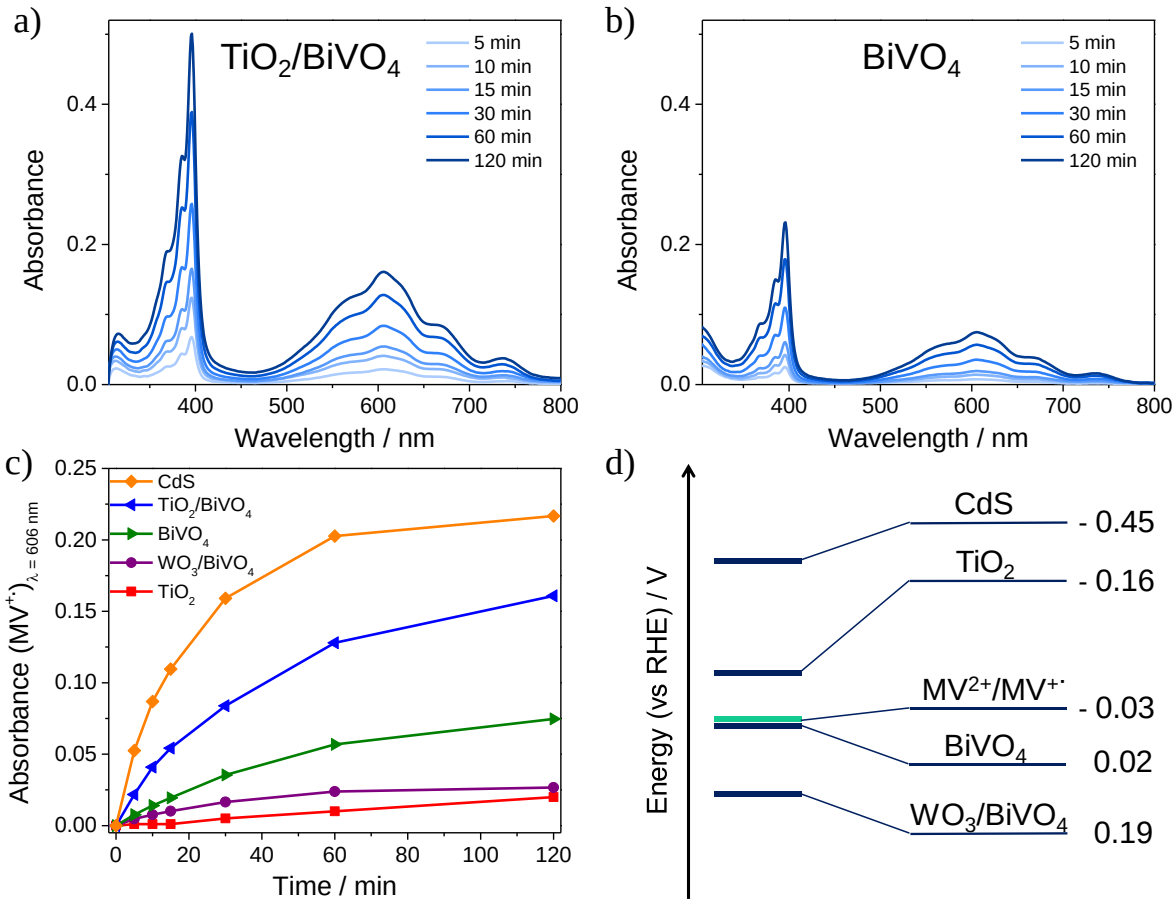

Fig. 7. Absorption spectra recorded during methyl viologen (MV^{2+}) photoreduction experiments in the presence of (a) the $TiO_2/BiVO_4$ heterojunction and (b) pure $BiVO_4$. (c) Kinetic profiles (maximum $MV^{+\cdot}$ absorbance at 606 nm *vs.* time plots) obtained with different semiconductor systems in photocatalytic MV^{2+} reduction tests. (d) CB energy scale of the tested semiconductor systems compared to the $MV^{2+}/MV^{+\cdot}$ reduction potential. All potential values are taken from the literature: see refs. [63] for CdS, [17] for TiO_2, [59,60] for $MV^{2+}/MV^{+\cdot}$, [15] for $BiVO_4$ and the WO_3/ $BiVO_4$ heterojunction.

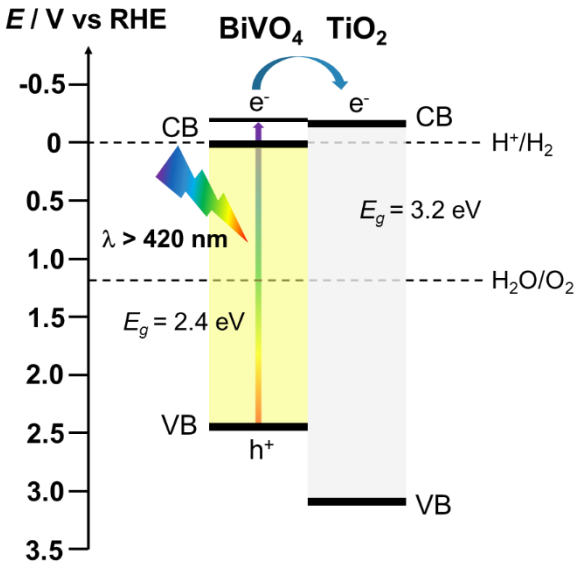

Fig. 8. Proposed electron injection mechanism for the $TiO_2/BiVO_4$ heterojunction under visible light irradiation.